Ceramics International 52 (2026) 735–747

Contents lists available at ScienceDirect

Ceramics International

journal homepage: www.elsevier.com/locate/ceramint

Valorizing carbonate-rich mining waste in porcelain stoneware production

Riccardo Fantini [a], Sonia Conte [b,*], Chiara Molinari [b], Chiara Zanelli [b], Michele Dondi [b], Maddalena Bernini [a], Alessandro F. Gualtieri [a], Rossella Arletti [a]

[a] Department of Chemical and Geological Sciences, University of Modena and Reggio Emilia, Via Giuseppe Campi 103, Modena, 41125, Italy
[b] CNR-ISSMC, National Research Council, Institute of Science, Technology and Sustainability for Ceramics, Via Granarolo 64, Faenza, 48018, Italy

ARTICLE INFO

Keywords:
Porcelain stoneware tile
Extractive waste
Carbonates
Technological properties
Microstructure

ABSTRACT

The increasing demand for raw materials in the ceramic tiles industry requires the exploration of secondary raw materials to mitigate the environmental impact of mining and quarrying, as well as to address waste management challenges. This study evaluates the potential of utilizing extractive waste generated from the washing of carbonate aggregates, taken from a quarry in Emilia-Romagna, Italy, in porcelain stoneware bodies. This waste was thoroughly characterized for its chemical, mineralogical, and thermal properties. It contains a high carbonate content (over 70 wt%) and was incorporated as a partial substitute for the fluxing components due to its low quartz content and limited plasticity. Laboratory scale tests were then performed on a reference batch (B0), two batches with simple substitution of 4 and 8 wt% of the fluxes with extractive waste (WS4 and WS8), and two batches with 4 and 8 wt% extractive waste and different proportions of all of the components (WF4 and WF8). Firing was performed from 1150 °C to 1230 °C to follow the evolution of the technological properties, phase composition (X-ray powder diffraction and the Rietveld method) and microstructure (SEM). No bottleneck was encountered in the tile-making process, but a delay in the sintering kinetics and a lower densification efficiency (from 2.391 g/cm^3 in B0 to 2.206 g/cm^3 in WS8) were observed in the fired products. The addition of waste silts induced a variation of the chemical composition of the batches that can lead to the production of porcelain stoneware tiles only with a careful batch design.

1. Introduction

Every year the ceramic tile industry requires a huge quantity of raw materials for worldwide manufacturing [1]. To limit the depletion of natural resources, a valuable and sustainable alternative is to introduce waste as a partial substitution for traditional raw materials. In this regard, the ceramic industry is effective in recovering and reusing its own residues, such as broken unfired or fired products and grinding scrap, while over the last few decades waste from other sectors is being evaluated and tested [e.g. 2,3]. The main obstacle to a widespread use of secondary raw materials is their unpredictable effect on the whole ceramic process, i.e. on the technological behavior and technical performance of the ceramic products, environmental impact, and economic sustainability [3]. In addition, the high heterogeneity of waste is another issue that the industry must face by implementing secondary raw materials into the production process. An in-depth characterization and laboratory scale testing from milling to firing of each waste-containing ceramic batch is thus mandatory to undertake the challenge of using secondary raw materials for ceramic tile manufacturing.

The extraction of ornamental stones and aggregates is important for the European economy. This activity generates extractive waste (EW) that includes irregular blocks, stone chips and residual sludge resulting from prospecting, extraction, treatment and storage of mineral resources and the working of quarries [4]. The management of this waste may represent more than 3 % of the operating costs of dimension stone working plants. In the EU, EW represents 20–30 % of the total waste production (up to 500–700 Mt/year, data from Eurostat), and it is thought that 5.9 billion tons of EW waste is stored within the EU [5].

There are at least two major issues linked to EW: i) the disposal of dumps and tailings has a significant impact on the landscape, with potentially negative effects on slope stability, hydrogeology, and aesthetic appeal of tourist destinations; ii) tailings may be contaminated by hazardous minerals/elements and/or chemicals. However, while the disposal of EW is non-compliant with the principles of the European Union, its recovery aligns perfectly with them in terms of waste recycling, resource conservation, and energy efficiency [6–9]. It is important

* Corresponding author. CNR-ISSMC, Institute of Science, Technology and Sustainability for Ceramics, via Granarolo 64, 48018, Faenza, Italy.
E-mail address: sonia.conte@issmc.cnr.it (S. Conte).

https://doi.org/10.1016/j.ceramint.2025.11.373
Received 25 August 2025; Received in revised form 10 November 2025; Accepted 25 November 2025
Available online 26 November 2025

to stress that waste also needs to be characterized in terms of health & safety and hence upgraded to secondary raw materials (SRM), considering possible pollutants and carcinogens such as asbestos, TPH (Total Petroleum Hydrocarbon), and heavy metals [5,9–13].

To undertake EW recycling, a comprehensive investigation is essential to estimate the volumes, size distribution, chemical and mineralogical characteristics of the material. The composition, grain size distribution, and rheological properties of EW are highly variable and significantly influence its technological properties and potential applications.

EW can be exploited for the recovery of minerals of industrial interest [6,14], metals [15,16] and critical raw materials (e.g. REE from Pb-Zn mine tailings [17]). The majority of the available literature is related to the recovery of minerals of industrial interest, due to their paramount economic importance. Quartz and feldspars for the glass and ceramic industry can be extracted from granite quarry waste thanks to specific mineralurgical treatments, e.g. crushing, sieving and magnetic separation [6]. Granite, clay tailings, and lime tailings were also tested as starting materials for the production of ceramic foams [18], mortars [19,20], and artificial soils [21].

Waste from dust suppression in dry mining and dressing plants deserves particular attention due to health & safety concerns. Similarly, sludges, clarified waters, and muds from filter press in wet machining may be revalued depending on their composition, safety, and throughput. Dry muds may be employed in brick kilns, or environmental restoration projects [8,22–24]. As an example, clayey quarry sludges generated during aggregate washing process were tested for the production of ceramic bricks [25] and tiles [26,27]. Moreover, high-field magnetic separation can be the most appropriate pre-treatment, both during waste characterization and industrial valorization [13].

Carbonate sludge (CS) from limestone quarrying has been tested as a substitute for more expensive ingredients in the building sector (e.g. concrete and ceramics), as an aggregate in open graded friction course (OFC), for acid mine drainage, and for erosion control in the restoration of limestone quarries [e.g. 7,10,23,28–34]. Calcium-rich raw materials (calcite, dolomite, wollastonite, diopside, etc.) have sometimes been used as sintering promoters in porcelain and porcelain stoneware tiles [32,35–42].

Previous studies demonstrated that achieving the goal of a “zero-waste-volume” in the lapidary and aggregate mining is theoretically possible by transforming dumps into “new mines”.

This paper is the outcome of a feasibility study conducted to evaluate the potential for the exploitation of sludge generated during the washing process of limestone aggregates. This waste contains significant amounts of carbonates and clay minerals and, in this case, instead of being used traditionally in the brick industry, it has been exploited for the production of porcelain stoneware tiles, partially replacing conventional raw materials. This application has been poorly undertaken previously, as carbonates are usually used as pore-forming agents in porous tiles.

2. Materials and methods

2.1. EW collection and characterization

EW was provided by CABE s.r.l. (Santarcangelo Di Romagna, Rimini). The company produces aggregates for building applications from the plant in Ripa Calbana quarry in Masrola (Borghi, Forlì-Cesena). Here, the aggregates are extracted from San Marino Formation, mainly constituted by organogenic limestone and calcarenites. The San Marino Formation consists of grey organogenic limestones and white-grayish calcarenites rich in bioclasts, including coral and bryozoan fragments. These rocks are intensely bioturbated and display concave-convex stratification, sometimes parallel, wavy, and cross-bedded with mega-ripples. The formation reaches a maximum thickness of 200 m and represents a marine platform depositional environment. The upper boundary is discordant with the Acquaviva Formation, composed of coarse bioturbated grey-yellowish sandstones, containing various sedimentary structures, such as cross and plane-parallel lamination and fluid escape structures. Subordinate lenticular conglomeratic layers are also present. The formation includes some pelitic levels, occasionally containing interbedded bituminous layers (Fig. 1).

The ore is loosened by blasting and is then moved to two different processing plants (Del Monte and Calbana) where crushing, washing and sieving occur. The treatment of the carbonate aggregates includes a washing process, after which, the resulting water undergoes a clarification phase, during which all effluents from the washing plant are subjected to flocculation and filtration using a filter press. The two clarification systems produce about 15–20 kt/year of waste silts (Fig. 2), which are temporary stocked into a dedicated area of the quarry. The humidity of the EW as extruded by the filter press is about 18–20 %, while the humidity drops to 8–10 % in 40–60 days of storage in an area protected from rain. The EW here studied derives from the carbonate aggregate washing process.

This EW is primarily silt classified as non-hazardous special waste under Italian legislation. It is typically used for restoration projects in the same quarry, as well as for excavation cavities, landfills, and other environmental restoration projects located outside the extraction site. Furthermore, this waste was utilized in the cement production of a local facility until its closure in 2009.

In this project, four samples of waste silts (WS) were considered: LI1a and LI1b collected from Del Monte plant, and LI2a and LI2b collected from Calbana plant. The -a and -b letter of the tags indicate that the samples were collected from lots produced in two different weeks. Representative specimens of the four samples were obtained by repeated coning and quartering, and these specimens (about 100 g) were then employed for all the following analyses, unless otherwise stated.

The chemical characterization of WS (as well as of the raw materials used for the batches formulation – not reported in this work) was performed by X-ray fluorescence analysis (XRF). XRF tablets were prepared by mixing 2.7 g of WS with 0.27 g of wax. The mixtures were then added into 40 mm aluminum molds with H_3BO_3 (approximately 6 g) as backing support for the tablet, and finally pressed at 15 tons. Data collection was performed by a Zetium wavelength-dispersive X-ray fluorescence spectrometer (Malvern Panalytical, Almelo, The Netherlands), equipped with a Rh X-ray tube. Data treatment was performed by using calibration curves of 54 certified silicate standards. Analyses are considered accurate within 2–5 wt% (relative) and the precision is estimated to the second decimal place.

The quantitative mineralogical analysis of the WS was performed using the Rietveld method [44] on X-ray powder diffraction (XRPD) data. Samples were finely ground in agate mortar and added with 10 wt % of corundum (α-Al2O3) NIST 676a as internal standard [45]. The specimens were then collected with the side loading technique at ambient conditions using a θ–θ Bragg-Brentano PANalytical X’Pert Pro Diffractometer, equipped with a real-time multiple strip (RTMS) detector (Cu Kα radiation, 40 kV, 40 mA), ½° divergence slit, ½° anti-scatter slit and 0.02 rad Soller slits. Besides the XRPD measurement on the raw waste, three iso-oriented samples deriving from the <2 μm fraction were also measured for better evaluation of the (00l) reflections of clay minerals. The <2 μm fraction was concentrated by the Stokes’ law. XRPD patterns were collected in the range 3–14 °2θ: 1) in air; 2) after thermal treatment at 550 °C for 30 min; 3) following ethylene glycol solvation overnight at 60 °C. Qualitative phase analyses were performed by the X’Pert High Score Plus software (PANalytical BV, Almelo, The Netherlands, [46]). Rietveld refinements were performed (on the side-loading data) using the GSAS package [47] and its graphical interface EXPGUI [48].

Thermogravimetric analysis (TGA) was performed with a Seiko SSC 5200 thermal analyzer (20 mg of sample; 10 °C/min heating rate; 25–1050 °C range).

As regards organic and inorganic carbon content, the total carbon (TC) content was measured by Elemental analyses using a Thermo-

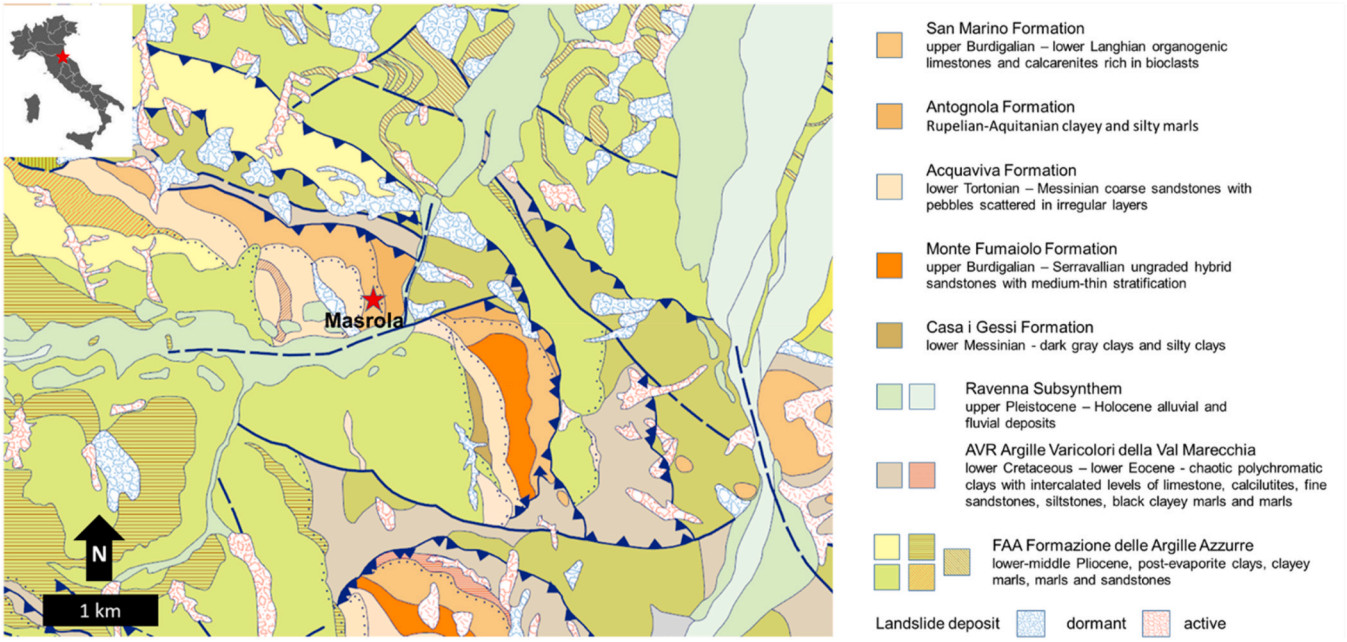

Fig. 1. Simplified geological map of the area surrounding the Ripa Calbana quarry in Masrola (Borghi, Forlì-Cesena) [43].

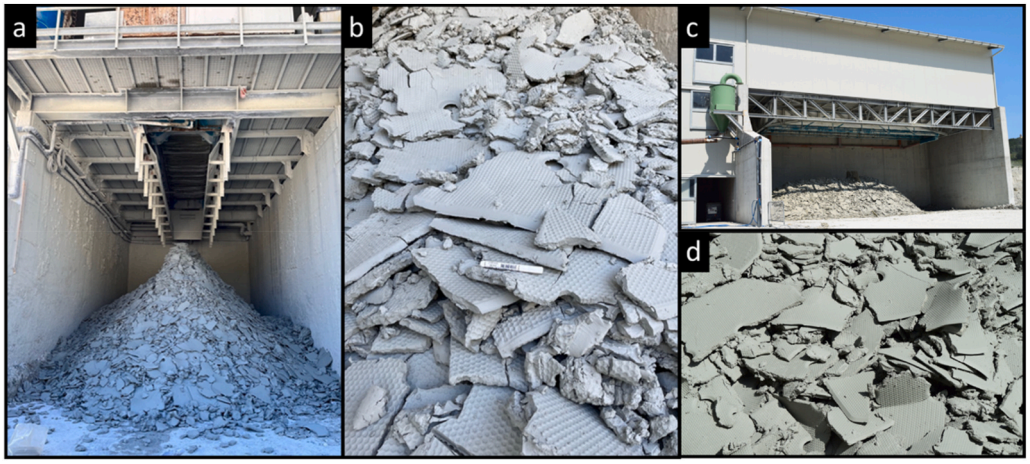

Fig. 2. Waste silts at the Del Monte (a, b) and Calbana (c, d) filter presses.

Fisher CHNS FLASH 2000 analyzer. Samples ranging from 0.7 mg to a few milligrams were analyzed for C and H content. The CO_2, and thus carbonate, content in the four WS was determined using the traditional gas volumetric method (calcimetry, ISO 10693:1995 [49]), allowing for total inorganic carbon (TIC) quantification. Total organic carbon (TOC) was then obtained as the difference between TC and TIC.

WS was also characterized by laser diffraction for particle size distribution using a Mastersizer 3000 laser grain-size analyzer. Hydro EV dispersion unit was used according to the reference standard ISO 13320:2020 [50] "Particle size analysis – Laser diffraction methods". A refractive index of 1.52 was used for the optical model. To evaluate the plasticity of the WS, Atterberg limits, as Plastic Limit (PL), Liquid Limit (LL), and Plastic Index (PI = LL-PL), were determined according to ISO 17892–12:2018 [51] standard.

Finally, the thermal behavior of WS was determined through hot-stage microscopy (HSM, TA Instruments, model ODP868) to verify its compatibility with a specific component of the ceramic body (plastic component, flux or skeleton). The hot-stage microscopy (HSM) experiment was carried out on cylindric specimens (3 × 1 mm, height × diameter, obtained using the specific instrument for the HSM) with a heating rate of 10 °C/min up to 1500 °C.

2.2. Batch formulations and laboratory-scale ceramic process

Ceramic batches were formulated based on the results of waste silt characterization. The waste silt is primarily composed of carbonates with minor silicate components. The content of quartz and clay minerals (the latter with low plasticity) is too low to replace either the skeleton or the plastic components of the ceramic body, respectively. Thus, the selected WS (LI2-a) was inserted in partial substitution of fluxes, also considering its thermal behavior (section 3.1). Indeed, CaO-rich raw materials are known to favor the sintering via the formation of eutectics and the crystallization of new phases such as anorthite, pyroxene and gehlenite [e.g. 36,37,52–55]. However, carbonates are also known to induce pore formation due to CO_2 release and are employed as a pore-forming agent in porous and lightweight ceramics [e.g. 38,56–58]. Hence, the attempt to use them in partial substitution of traditional raw materials in porcelain stoneware tiles required a correct reengineering

of the ceramic batch.

In this work, five batch formulations were designed: one benchmark (**B0**, no waste); two batches with a high amount of waste silt (4–8 wt%) as a simple replacement for conventional fluxes (**WS4, WS8**); two other batches with the same amount of waste silt (4–8 wt%), but changing the entire batch formulation in order to bring the final chemical composition as close as possible to that of the benchmark (**WF4, WF8**). The formulation of the designed batches and their calculated chemical composition are shown in Table 1. Concerning the benchmark B0, it must be stressed that, besides being close to traditional porcelain stoneware batches, some peculiar raw materials were employed. In fact, the current crisis of the classic raw materials used for the production of porcelain stoneware is forcing the industrial community to find solutions to mitigate the supply risk. In this sense, the use of local raw materials could be one of the answers to adopt. Therefore, in this benchmark a locally sourced potassium flux together with the classic Turkish sodium one was used. The batches so formulated underwent the simulation of the industrial tilemaking process at the laboratory scale. The raw materials were ball milled in a porcelain jar using dense alumina grinding media, 40 wt% water (by weight of the slip) and 0.3 wt % deflocculant (sodium tripolyphosphate) by weight of dry batch, for 25 min. The slips were oven dried, de-agglomerated using a hammer mill with grid of 500 μm and manually granulated by exploiting a 2 mm sieve with moisture ~8 wt %, as used in the industrial practice. Powders were pressed (40 MPa) into 50 mm diameter discs and then oven dried at 105 °C overnight. Following this, powder compacts were tested with HSM – the same used for pristine waste silt – with a thermal cycle ranging from room temperature up to 1400 °C, with a heating rate of 40 °C/min and 5 min of dwell time. HSM registered the size variation of a 5 × 5 × 5 mm chip cut from the dry samples, determined by the pixel count during the thermal cycle. This allowed comparison of the sintering behavior of the batches containing the waste silt with respect to the benchmark. Powder compacts were then fast fired in an electric kiln (PKP-ERO, Nannetti, Faenza, Italy) at different maximum temperature from 1150 °C up to 1230 °C, to follow the technological properties of the tiles over a range of firing temperatures from an incomplete sintering to overfiring conditions. The thermal cycle consisted in a 60 min cold-to-cold cycle with 5 min of dwell time at T_{max}.

Table 1
Formulation of the designed batches and their calculated chemical compositions. The chemical composition of the ceramic batches was calculated based on that of the raw materials and carbonate waste, as determined by XRF-WDS, taking into account the weight contribution of each raw material and waste to the overall body formulation.

Raw material wt.%	BATCH				
	B0	WS4	WS8	WF4	WF8
ball clay 1	25	25	25	16	10
ball clay 2	15	15	15	15	15
kaolin	–	–	–	9	15
sodic feldspar	35	35	35	30	20
K-feldspar sand	20	17	14	10	12
quartz/feldspar sand	3	2	1	6	8
quartz	2	2	2	10	12
waste silt	–	4	8	4	8
Total	100	100	100	100	100
Calculated chemical composition					
SiO_2	70.96	68.95	66.93	69.62	67.63
TiO_2	0.57	0.57	0.57	0.46	0.41
Al_2O_3	20.05	19.85	19.64	20.12	20.28
Fe_2O_3	0.61	0.69	0.76	0.70	0.81
MgO	0.40	0.49	0.57	0.45	0.57
CaO	0.66	2.93	5.21	2.90	5.27
Na_2O	4.22	4.18	4.13	3.60	2.60
K_2O	2.53	2.36	2.19	2.15	2.43
Total	100	100	100	100	100
Alumina Saturation Index (ASI)	1.84	1.35	1.05	1.49	1.23

2.3. Characterization of semi-finished and finished ceramic products

The technological behavior of semi-finished products was appraised through the determination of the following characteristics: particle size distribution by X-ray monitoring of gravity sedimentation (Micromeritics, SediGraph 5100) (ASTM C958-92 [59]); powder moisture (ASTM C324-01 [60]); green and dry bulk density (weight/volume ratio); springback after pressing (i.e. $100(D_p\text{-}D_m)/D_m$, where D_p is the diameter of the pressed tile and D_m is the diameter of the mold).

After firing, the measured technological properties for all the bodies were: linear firing shrinkage (i.e. $100(D_m\text{-}D_f)/D_m$ where D_f is the diameter of the fired discs and D_m is the diameter of the mold), water absorption, bulk density and open porosity (ASTM C373-18 [61]). The samples fired at the temperature of maximum densification (T_{md}) were further investigated: CIE-Lab colorimetry (ISO 10545-16 [62], MSXP-4000; Hunterlab, Reston, VA, USA) to get L^*, a^*, and b^* coordinates; mineralogical quantitative analyses (performed as described in section 2.1 for pristine WS). For the determination of the flexural strength (ASTM C648-20 [63]), tiles of 110 × 55 × 5 mm were obtained with a hydraulic press (40 MPa) and fired at the temperature of T_{md} before testing.

Moreover, the microstructure of selected samples was investigated by scanning electron microscopy (SEM) on polished samples in epoxy resins. For a better description of the mineral phase assemblages formed during firing, the surface of some specimens was etched for 4 min with a 15 % HF solution, ultrasonically washed with distilled water and dried. In both cases, after carbon coating, the SEM analyses were carried out using a JSM-6010 LA InTouchScope (JEOL, USA) equipped with a silicon-drift energy dispersive X-ray spectroscopy (EDS) detector (energy resolution: 133 eV or better). Images were mainly performed by the backscattered electron detector.

Table 2
Chemical composition of carbonate sludges from XRF measurements. N.d. = not detected.

	LI1-a	LI1-b	LI2-a	LI2-b
Major Elements (wt.%)				
SiO_2	15.78	16.02	16.24	14.77
TiO_2	0.19	0.19	0.20	0.19
Al_2O_3	5.86	5.83	5.78	5.32
Fe_2O_3	1.41	1.39	1.55	1.37
MgO	1.55	2.40	1.80	2.84
CaO	37.90	36.79	38.02	38.59
Na_2O	0.16	0.16	0.19	0.18
K_2O	1.13	1.13	1.14	1.05
P_2O_5	0.29	0.30	0.26	0.28
S	0.10	n.d.	0.13	0.13
L.O.I. (Loss on Ignition)	35.50	35.60	34.59	35.18
Total major and minor oxides	99.87	99.81	99.89	99.9
Trace Elements (ppm)				
Cl	126	112	117	153
Zr	n.d.	77	75	84
MnO	362	299	346	286
Ni	45	n.d.	55	59
Zn	57	65	85	66
Rb	39	31	41	38
Sr	297	327	335	357
Y	10	16	10	10
Ba	140	n.d.	n.d.	n.d.
Cr	127	n.d.	50	n.d.
Cu	n.d.	38	n.d.	n.d.
S	n.d.	967	n.d.	n.d.
W	66	n.d.	n.d.	n.d.
Total	100.00	100.00	100.00	100.00

3. Results and discussion

3.1. Characterization of waste silts

Chemical data of waste silt samples obtained by XRF are reported in Table 2. All of them display very similar compositions, poor in silica (14.77–16.24 wt%) and alumina (5.32–5.86 wt%), rich in CaO (36.79–38.59 wt%), with minor content of MgO (1.55–2.84 wt%), Fe_2O_3 (1.37–1.55 wt%) and K_2O (1.05–1.14 wt%), also showing values of TiO_2, Na_2O, P_2O_5 and S well below 1 %. Similarly, most trace elements are below 100 ppm, with the exception of Cl (112–153 ppm), MnO (286–362 ppm), Sr (297–357).

Qualitative and quantitative mineralogical compositions were obtained by coupling TGA, calcimetry, EA, and XRPD. Results on the quantification of carbonates from XRPD are reported in Table 3 (together with the full mineralogical analysis), while results from calcimetry and TGA are reported in Table 4 and Fig. 3.

All WS display high levels of carbonates (75–82 wt%), mostly represented by calcite and dolomite/ankerite. It is noteworthy that the total carbonates content from XRPD (Table 3) is coherent with calcimetry and TGA data (Table 4), even if a slight overestimation of carbonates from XRPD seems to occur. Merging carbonate quantification from calcimetry and elemental analysis it is possible to calculate TC, TIC and TOC values, highlighting the almost complete absence of organic carbon in the WS (TOC below 0.25 %, Table 5).

XRPD on oriented specimens (Fig. 1S, supplementary materials) highlighted the presence of a small fraction of clay minerals (also confirmed by TGA) such as mica (possibly glauconite-illite more than muscovite), kaolinite, and I/S mixed layers. The latter, expandable clays were not quantified due to their signal being too weak in the random oriented XRPD pattern. Examples of graphical outputs of Rietveld refinements are provided as Fig. 2S (supplementary materials). The mineralogical analyses match the geological setting of San Marino Formation of the area of the quarry.

The particle size distribution of the waste silts is reported in Fig. 3S (supplementary materials), showing the frequency distribution and cumulative volume at each size class. All the samples display a trimodal distribution, with the two major components at about 30 and 5 μm and a minor component below 1 μm. Thanks to the fine-grained distribution and a fair content of clay minerals, the WS has a certain plasticity (the Atterberg limits are, on average, LL = 34.9 ± 2.8; PL = 21.8 ± 1.6; PI = 13.1 ± 1.4; Table 6).

The results reported above highlighted a high homogeneity of the analyzed samples, both in "time" (slight differences between –a and –b batches) and "space" (slight differences between LI1 and LI2). This is an important preliminary result in view of future implementation, indicating that WS coming from the two plants and from different operating periods may be mixed to obtain a larger, homogeneous batch.

Table 3
Results of the quantitative phase analysis from XRPD data using the Rietveld method.

Rietveld agreement indices[a]	LI1-a	LI1-b	LI2-a	LI2-b
R_{wp} (%)	9.02	9.72	11.67	11.16
R_p (%)	6.75	7.32	8.84	8.55
χ^2	1.922	2.195	3.161	2.838
Phases (wt.%)				
calcite	79.6 ± 1.6	69.4 ± 1.4	74.5 ± 1.5	71.5 ± 1.4
dolomite/ankerite	1.2 ± 0.1	5.3 ± 0.3	6.1 ± 0.2	10.6 ± 0.4
quartz	4.2 ± 0.1	3.4 ± 0.1	4.7 ± 0.1	3.5 ± 0.1
K-feldspar	1.3 ± 0.2	0.9 ± 0.1	2.1 ± 0.2	1.3 ± 0.2
plagioclase	2.0 ± 0.2	–	2.6 ± 0.2	–
pyroxene	–	3.7 ± 0.5	–	4.6 ± 0.6
kaolinite	2.3 ± 0.2	2.6 ± 0.4	1.6 ± 0.3	1.3 ± 0.3
glauconite	2.2 ± 0.2	–	2.7 ± 0.3	–
mica	6.9 ± 0.4	14.7 ± 0.3	5.9 ± 0.6	7.1 ± 0.5

[a] The definition of the agreement indices is taken from Larson & Von Dreele [47].

Table 4
Carbonate quantification from calcimetry and thermogravimetric analysis. Calcite stoichiometry was employed for quantification, since it is not possible to discriminate the ankerite contribution. For TGA, only weight losses between 400 and 1000 °C were considered.

Carbonates wt.%	LI1-a	LI1-b	LI2-a	LI2-b
Calcimetry	74.4	73.9	75.0	77.2
TGA	75.9	76.3	74.5	78.6

Sample LI2-a has been selected to study its thermal behavior by hot stage microscopy test (Fig. 4). It shows a limited volume contraction at about 800 °C, immediately followed by a limited bloating stage. When the temperature increases to ~1245 °C, sintering begins to reach maximum densification at ~1450 °C. When compared with a classical Turkish feldspar used in the ceramic industry as a flux, it can be seen that limestone needs a higher temperature to activate sintering and bring it to completion (~150 °C higher than feldspar). It can be inferred that WS does not have excellent fluxing properties; however, as mentioned above, Atterberg tests indicated very low plasticity, ruling out the possibility of using WS as a plastic component of the batch. Therefore, it was decided to use limestone silt (sample LI2-a) as a partial replacement for feldspars and quartz/feldspar sand in the ceramic body.

3.2. Ceramic bodies characterisation

The chemical composition of the ceramic bodies (Table 1) indicates that in WS4 and WS8 (batches with waste silt in simple replacement for conventional fluxes), the addition of waste results in a decrease in silica and alumina content, accompanied by a significant increase in Ca, while the Na and K concentrations are kept close to those of the benchmark. Specifically, the introduction of waste silt, which consists of approximately 70 % calcite (CaO ~40 %), induces a change in the chemical composition of the ceramic body from distinctly peraluminous (ASI 1.84) towards the peralkaline field (down to 1.05 for WS8). This shift may lead to technological problems, such as reduced densification efficiency and potential bloating phenomena [64–66]. Consequently, the two other batches (WF4 and WF8) were formulated by adjusting the ratios of all components to align the chemistry as closely as possible with that of the reference body (Fig. 4S, supplementary materials).

The particle size distribution of the slips after wet grinding (Fig. 5) is similar for all batches and perfectly matches the industrial practice (orange area in the Figure). In fact, the d_{50} (Table 7) slightly decreased in the presence of WS in the straightforward substitution of feldspars and quartz sand (~3.8 μm for WS4 and WS8 *vs* 4.0 μm of the benchmark), and slightly increased in the fully modified batches (4.1 μm for WF4 and WF8), as a result of the higher quartz content (Table 1).

The other values reported in Table 7 indicate that the presence of the WS did not significantly modify the technological properties of unfired porcelain stoneware samples during the various steps of the tile production: granulation, shaping and drying steps. Indeed, the small variations observed correspond to the range usually accepted in industrial practice.

Results of HSM tests are shown in Fig. 6. The benchmark (black curve) presents a typical trend of porcelain stoneware, characterized by a progressive shrinkage (corresponding to sample densification) up to a maximum, without abrupt changes in the curve, followed by expansion. Otherwise, all batches containing WS exhibit a plateau between 1000 °C/1100 °C, where densification is frozen, probably related to crystallization of newly formed phases, coherently with the high amount of calcium introduced by the WS. Actually, this plateau is more evident in mixtures with 8 % WS, likely indicating a higher phase crystallization

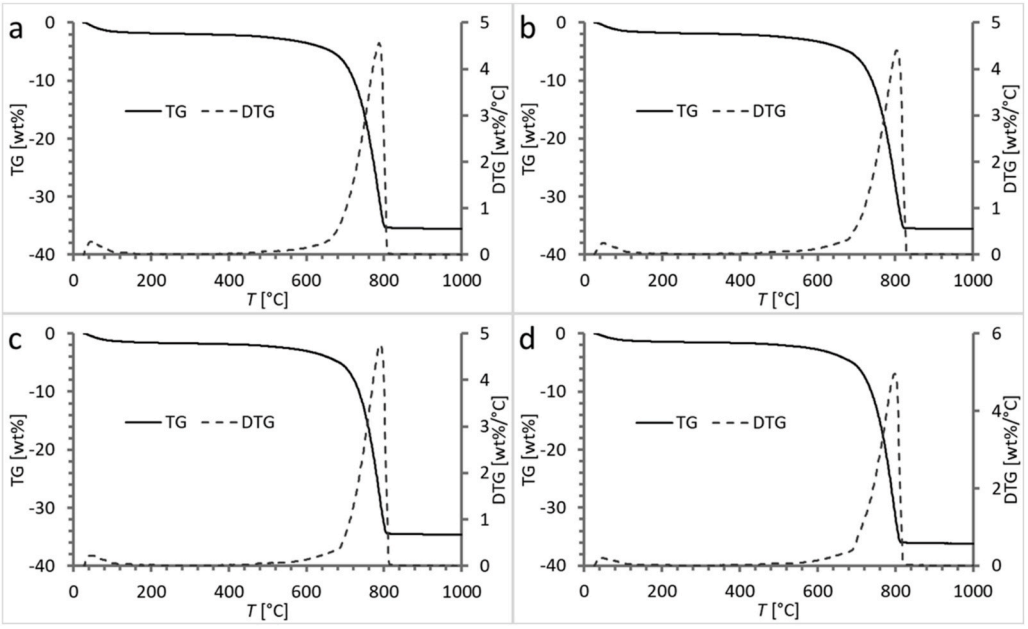

Fig. 3. Thermogravimetric analyses of carbonate sludges from a) LI1-a; b) LI1-b; c) LI2-a; d) LI2-b.

Table 5
Carbon content of the waste silts. Total carbon (TC) from elemental analysis, total inorganic carbon (TIC) from calcimetry, total organic carbon (TOC) with TOC = TC-TIC. The slightly negative value of TOC for LI2-a simply indicates the absence of organic carbon.

wt.%	TC	TIC	TOC
LI1-a	9.03	8.92	0.11
LI1-b	9.12	8.87	0.25
LI2-a	8.93	8.99	−0.06
LI2-b	9.41	9.26	0.15

Table 6
Atterberg limits of waste silts.

wt.%	Liquid limit	Plastic limit	Plasticity index
LI1-a	36.7	23.3	13.4
LI1-b	37.7	22.9	14.8
LI2-a	33.3	21.1	12.2
LI2-b	31.7	19.9	11.8
average	34.9 ± 2.8	21.8 ± 1.6	13.1 ± 1.4

compared to mixtures containing 4 % WS. Subsequently, the incipient melting of feldspars (which begins at about 1000 °C) prevails over crystallization, and the densification process takes place.

The onset of crystallization induced a delay in the sintering process for WS-bearing batches that has already been observed in the literature, both through *ex-situ* tests [55] and *in-situ* analyses [37,38,67]. In particular, the HSM tests showed that an increasing amount of calcite added to a porcelain stoneware body (Fig. 4 [67], Fig. 2a [37]) and to a lightweight ceramic (Fig. 3 [38]), resulted in the crystallization of Ca-rich phases, with a clearly visible plateau in the densification curves and a consequent shift in the temperature at which fast sintering kinetics took place.

Another parameter that can be investigated through the sintering curves is the densification efficiency. When comparing the WS-bearing bodies created with a simple replacement of feldspar (dotted lines) to those where the entire formulation was redesigned (solid lines) at the same waste content, it is evident that the volumetric shrinkage is greater for the latter. This indicates that, with equal WS content, the densification efficiency will be higher in WF4 and WF8 than in WS4 and WS8. Consequently, the bulk density of the fired tiles will be greater.

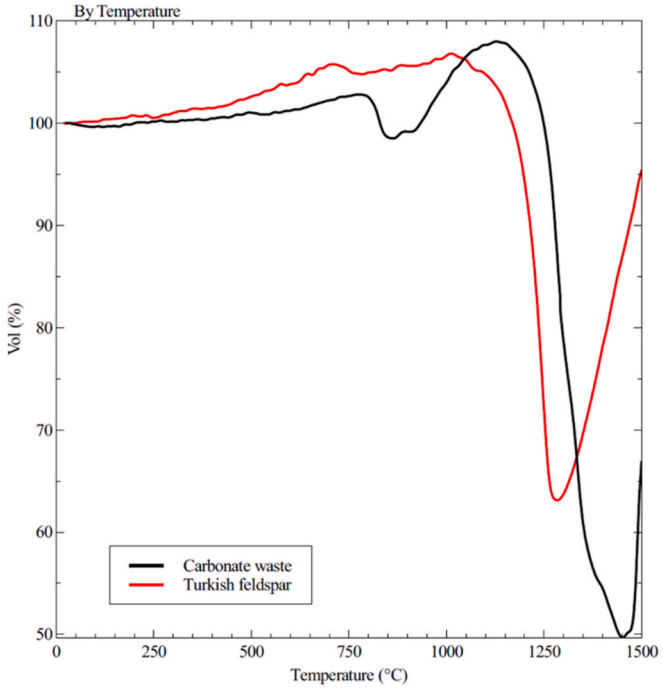

Fig. 4. Thermal behavior of the waste silt compared to a classic Turkish feldspar.

Based on the information gained from HSM tests, the batches were fast fired at different maximum temperatures. The gresification curves of the ceramic batches, obtained by the values of water absorption and bulk density, are reported in Fig. 7. Unlike the semi-finished products, the presence of the WS significantly influenced the firing behavior – as just discussed for the sintering curves – and the technological properties of the finished products (see Table 8 for the properties at T_{md} and Table 1S, supplementary materials, for all the temperatures).

Considering the gresification curves, it can be observed that the

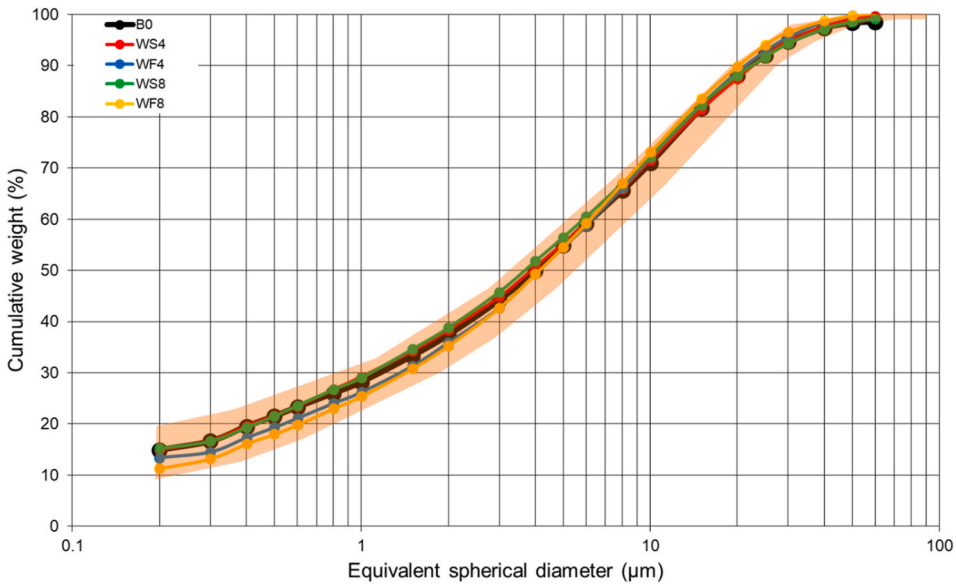

Fig. 5. Particle size distribution of batches obtained by X-ray monitoring of gravity sedimentation. The orange area indicates the typical distributions in the industrial practice.

Table 7
Technological properties of unfired products.

Property	B0	s.d.	WS4	s.d.	WS8	s.d.	WF4	s.d.	WF8	s.d.
Slip particle size d_{50} (μm)	4.0	0.1	3.9	0.1	3.7	0.1	4.1	0.1	4.1	0.1
Powder moisture (% wt.)	7.7	0.2	7.9	0.1	7.8	0.2	7.4	0.3	7.7	0.2
Springback (cm/m)	0.48	0.06	0.44	0.04	0.43	0.04	0.53	0.06	0.46	0.03
Green bulk density (g/cm^3)	2.134	0.005	2.160	0.003	2.183	0.020	2.129	0.009	2.163	0.007
Dry bulk density (g/cm^3)	2.003	0.030	2.005	0.006	2.032	0.020	1.987	0.008	2.007	0.005

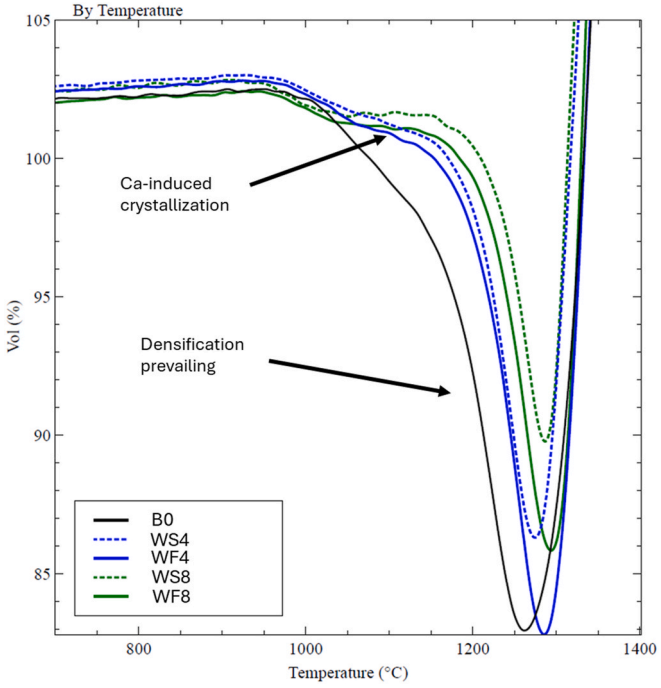

Fig. 6. Thermal behavior of ceramic batches.

benchmark achieved a high bulk density and a very low water absorption at 1170 °C, a temperature quite low with respect to a classic porcelain stoneware body. This may be due to the peculiar raw materials used for its formulation. Indeed, the addition to K-rich flux induced a lowering of the optimal firing temperature, coupled with a very good stability of the ceramic body [68].

As for the batches containing waste silt, its introduction increased the maximum densification temperatures for all batches, as previously observed in the HSM curves. This increase is particularly evident in WF4 (1200 °C) and WF8 (1220 °C), compared to WS4 (1190 °C) and WS8 (1210 °C). Indeed, in WF4 and WF8, the redesign of the entire formulation enhanced the presence of refractory phases, such as kaolinite and quartz (Table 1). Consequently, in addition to the delay caused by the crystallization of the Ca-rich phases, the presence of these refractory minerals further elevated the temperature. Despite this side effect, the modifications made in WF4 and WF8 successfully restored the technological properties of the benchmark, particularly in terms of bulk density. As illustrated in Fig. 7, the primary drawback of using this type of waste is the reduced densification efficiency, resulting in values lower than those of the benchmark. In this context, the alteration of the entire chemical composition of the batches enabled a recovery of density compared to the mixtures designed with only feldspar replacement: 2.336 g/cm^3 of WF4 batch *vs* 2.304 g/cm^3 of WS4, 2.258 g/cm^3 of WF8 *vs* 2.206 g/cm^3 of WS8. Furthermore, it is noteworthy that all samples exhibited good stability once the maximum densification temperature was surpassed, indicating a low tendency toward pyroplastic deformation. This extension of the dimensional stability temperature range, which offers a high degree of process control in the firing phase, has also been emphasised for lightweight ceramics with the addition of limestone [38].

With regard to other technological properties, the LS corroborates the HSM data and is clearly related to bulk density. Given the nearly identical initial density of the unfired material (as shown in Table 7), a lower LS corresponds to a lower bulk density of the fired samples. The

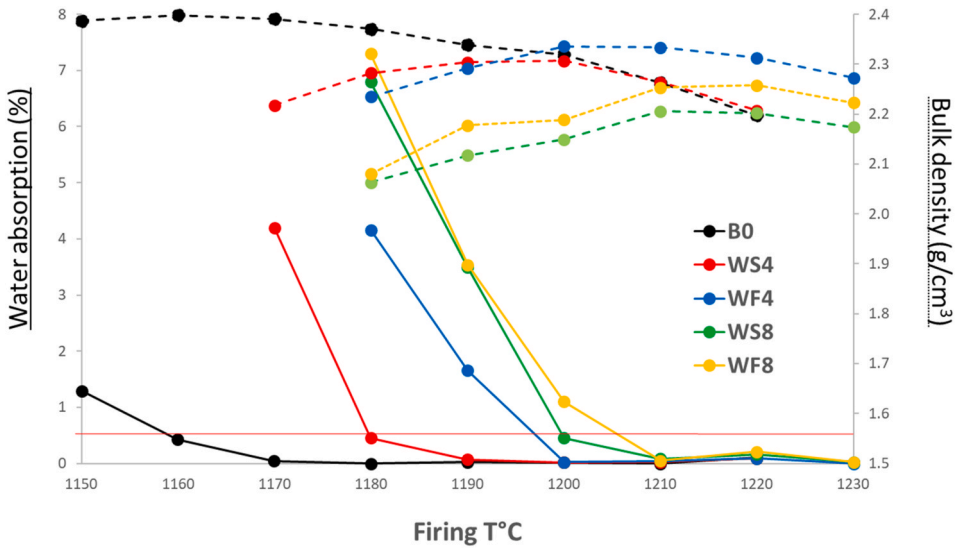

Fig. 7. Gresification curves of ceramic batches. Water absorption (solid lines) and bulk density (dashed lines) at the different maximum firing temperatures for each batch. The horizontal solid red line represents 0.5 % of water absorption. Experimental error is within the symbol size.

Table 8
Technological properties of fired products at the T_{md}. T: firing temperature; LS: linear firing shrinkage; WA: water absorption; BD: bulk density; OP: open porosity; FS: flexural strength.

	Unit	B0	WS4	WF4	WS8	WF8
T	°C	1170	1190	1200	1210	1220
LS	cm/m	5.51 ± 0.01	4.16 ± 0.06	4.91 ± 0.02	2.63 ± 0.01	4.20 ± 0.01
WA	wt.%	0.04 ± 0.01	0.07 ± 0.03	0.02 ± 0.03	0.08 ± 0.02	0.21 ± 0.03
BD	g/cm^3	2.391 ± 0.001	2.304 ± 0.004	2.336 ± 0.004	2.206 ± 0.020	2.258 ± 0.002
OP	vol%	0.11 ± 0.01	0.16 ± 0.07	0.05 ± 0.08	0.18 ± 0.05	0.47 ± 0.06
FS	MPa	49.8 ± 2.9	45.3 ± 2.5	51.9 ± 0.2	50.2 ± 3.8	50.6 ± 3.1

OP at the gresification temperature is very low across all batches, reflecting the low water absorption. The FS measured at T_{md} improved in the batches containing WS compared to the reference body (except for sample WS4). Notably, WF4 achieved the highest performance at 51.9 MPa. This beneficial effect of WS addition can be attributed to mineralogical and textural changes in the fired products, as discussed below. In particular, this concerns the crystallization of calcic plagioclase, which has been shown to enhance FS in other ceramics, such as porous tiles [69], lightweight ceramics [38], porcelain and porcelain stoneware [35,37,39].

Table 9 shows the quantitative mineralogical composition of each final product at the different gresification temperatures. As expected at T_{md}, the main constituents of the benchmark are residual quartz and feldspar (with traces of rutile) together with the newly formed mullite and amorphous phase.

The mineralogical assemblage of the bodies containing the waste silt is similar to the reference, but the XRPD patterns and quantitative results reveal the formation of calcic plagioclase during firing (Fig. 8) and a decrease of mullite and quartz content. The decrease of quartz in finished products is currently a topic of paramount interest to the ceramic industry, in relation to the possible respirability of crystalline silica during drilling and cutting operations. In this sense, this result, i.e. the quartz lowering through the introduction of crystallization promoters, can certainly be a strategy to be pursued on an industrial scale [70].

The formation of calcic plagioclase is also confirmed by SEM analysis

Table 9
Quantitative phase analysis of tiles at the gresification temperature from XRPD data using the Rietveld method.

	B0-1170 °C	WS4-1190 °C	WF4-1200 °C	WS8-1210 °C	WF8-1220 °C
Rietveld agreement indices[a]					
R_{wp} (%)	6.74	6.08	6.41	5.72	6.57
R_p (%)	4.55	4.32	4.47	4.28	4.62
χ^2	7.278	5.651	6.388	4.929	6.574
Phases (wt.%)					
quartz	19.2 ± 0.2	14.2 ± 0.1	16.2 ± 0.1	10.7 ± 0.1	17.8 ± 0.1
sodic plagioclase (Ab)	15.3 ± 0.2	17.8 ± 0.3	13.6 ± 0.2	15.5 ± 0.3	11.6 ± 0.4
mullite	9.5 ± 0.3	5.9 ± 0.2	7.4 ± 0.2	2.6 ± 0.2	6.5 ± 0.3
rutile	0.2 ± 0.1	0.1 ± 0.1	0.1 ± 0.1	0.1 ± 0.1	0.1 ± 0.1
calcic plagioclase (An)	–	10.9 ± 0.3	9.2 ± 0.3	19.7 ± 0.3	16.4 ± 0.3
amorphous phase	55.8 ± 0.4	51.1 ± 0.5	53.5 ± 0.5	51.4 ± 0.5	47.6 ± 0.6
TOTAL	100.0	100.0	100.0	100.0	100.0

[a] The definition of the agreement indices is taken from Larson & Von Dreele [47].

of fired products, especially on the HF-etched sample. Fig. 9, indeed, shows crystals of anorthite and mullite in the WS8 body fired at 1210 °C, while some other SEM micrographs and EDS analyses are reported in Fig. 5Sa-c (supplementary materials).

As already mentioned, the formation of anorthite in CaO rich systems is well reported in various ceramic materials, especially in porous tiles or anorthite-based porcelain such as bone china tableware. In these systems anorthite is often found to be the most stable among the calcium silicates and aluminosilicates forming during heating [35,40,69,71]. For example, González-García and coworkers [72] reported how the formation of anorthite is favored from a thermodynamical viewpoint compared to that of larnite (Ca_2SiO_4), wollastonite (β-$Ca_2Si_2O_6$) and gehlenite ($Ca_2Al_2SiO_7$), and even of mullite, consistently with what observed for our samples, where the crystallization of anorthite is accompanied by a lowering in the mullite amount.

Concerning the significant lowering of quartz detected in WS4 and WS8, SEM analyses show quartz grains with evident reaction rims close to calcic plagioclase (Fig. 10). The reactivity of quartz with CaO is well

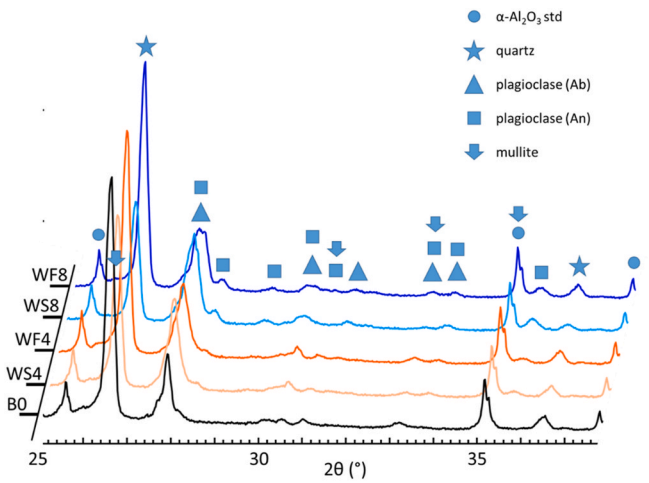

Fig. 8. X-ray powder diffraction patterns of fired products at the gresification temperature.

established in the literature with, e.g., quartz and alumina being mixed together with calcite to synthesize anorthite [41].

To highlight the relationship between quartz dissolution and anorthite crystallization, it can be considered that the amount of silica consumed by the crystallization of calcic plagioclase (considering a 44.4 % by weight of SiO_2 in anorthite) is perfectly equal to the quartz loss in batches WS4 and WS8 with respect to B0 (Table 10).

Furthermore, the chemical trends in Fig. 10 suggest that quartz

Table 10
Comparison between quartz in B0 and sum of quartz and silica in calcic plagioclase (An) in the WS containing batch. Calculations consider a SiO_2 content in anorthite of 44.4 wt%.

Quartz and plagioclase (An) content from XRPD					
	B0	WS4	WF4	WS8	WF8
quartz	19.2	14.2	16.2	10.7	17.8
plagioclase (An)	0.0	10.9	9.2	19.7	16.4
Total silica calculation					
SiO_2 from quartz (100 % of phase wt%)		14.2	16.2	10.7	17.8
SiO_2 in plagioclase (An) (44.4 % of phase wt.%)		4.8396	4.0848	8.7468	7.2816
quartz + SiO_2 in An		19.0396	20.2848	19.4468	25.0816

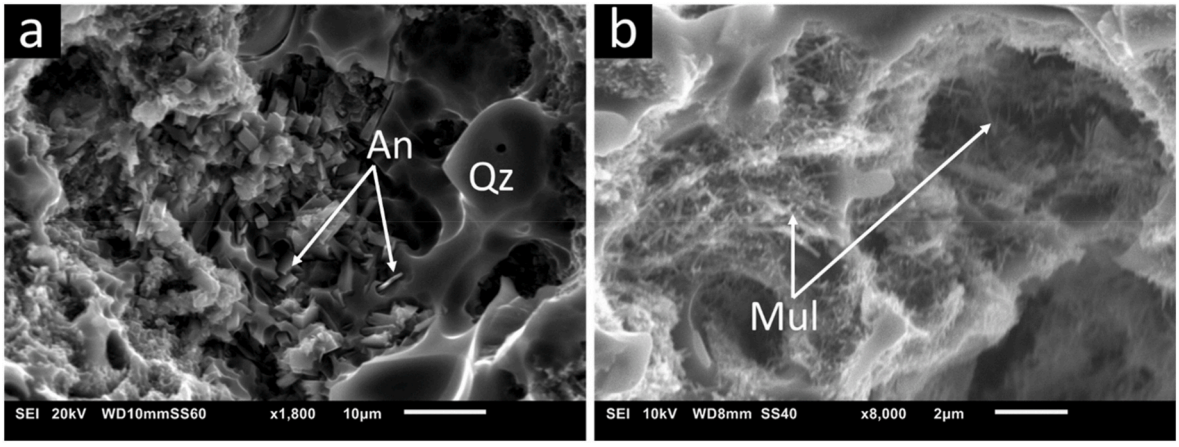

Fig. 9. Secondary electrons SEM micrographs of neo-formed phases in HF-etched WS8 at 1210 °C. a) Sharp crystals of calcic plagioclase at the boundary of a quartz grain. b) Mullite crystals in the amorphous matrix. The identification was made by EDS (see also Fig. 5Sa-b and Fig. 6S, supplementary materials).

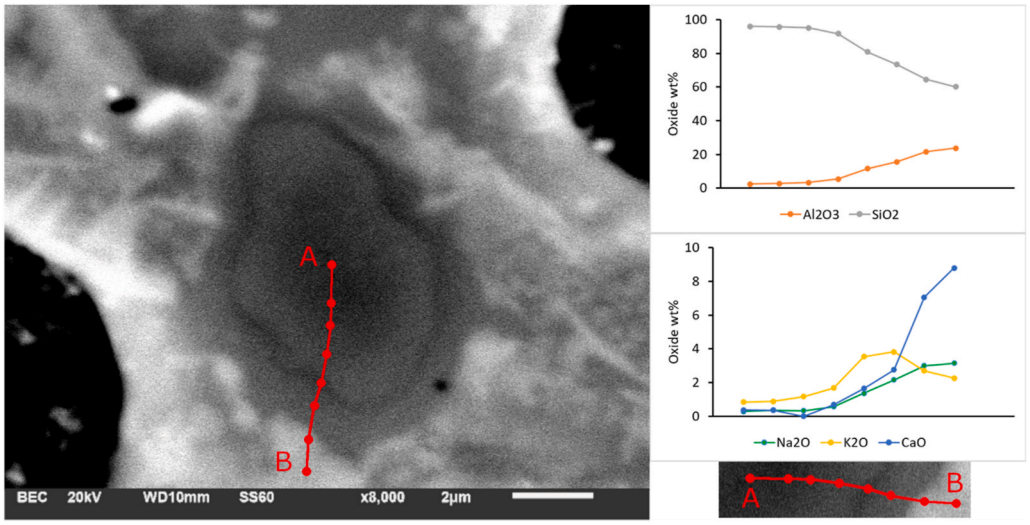

Fig. 10. SEM micrograph of a quartz grain with evident reaction rims in WS8 fired at 1210 °C. Diagrams on the right show the EDS evolution by moving from the center of the quartz grain (A) towards the matrix and finally a calcic plagioclase crystal (B).

interacts with the Al-K-rich matrix formed by flux melting, resulting in the crystallization of calcic plagioclase upon contact with the waste silt. Indeed, moving from the center of the quartz grain (A) towards the calcic plagioclase crystals (B), a progressive increase in Al, K, Na and, finally, Ca can be observed. It is also interesting to note how K_2O concentrates in the rim in between quartz and the newly formed plagioclase, according to the low solubility of K in anorthite [73]. The phase composition of WF4 and WF8 is close to that of WS4 and WS8. However, changes made in the formulation were effective in partially restoring quartz and mullite content of the bodies by increasing them, and, on the other hand, lowering both residual plagioclase and newly formed anorthite.

The microstructure of the bodies fired at the maximum densification and in overfiring conditions was studied by SEM analyses. Fig. 11 shows SEM micrographs of the five bodies at the gresification temperature. In these conditions, all the batches display a homogeneous and generally compact microstructure. In particular, B0 shows relicts of quartz and plagioclase (dark grey areas) surrounded by a light-grey vitreous (amorphous) phase. Pores (black areas) are generally rounded and span in size from few up to ~20 μm in diameter, with some more irregular and larger ones deriving from powder compaction defects, mainly associated with relicts of kaolinite flakes now completely transformed in mullite (e.g. Fig. 5Sc, supplementary materials).

Both samples containing 4 % of WS show microstructures quite similar to the benchmark, but with slightly higher porosity. The latter is much more abundant in the two batches containing 8 % of WS. In terms of pore size, all bodies that contain WS exhibit larger, rounded pores that are frequently surrounded by high-scattering halos, in addition to small pores and compaction pores. At higher magnifications, these halos display concentrated anorthite crystals that should derive from WS relicts (see also Fig. 5Sb, supplementary materials).

The origin of increased porosity in the WS-bearing batches is clearly related to the presence of carbonate in these bodies. Indeed, although carbonate decomposition (with CO_2 release) occurs before the onset of viscous flow and thus in a matrix that is still gas permeable, residual porosity may occur due to volume contraction related to decarbonation. This porosity is usually small in size [56]. On the other hand, the larger, rounded pores surrounded by high-scattering halos are consistent with the anorthite crystallization process. This feature is known in the literature as crystallization-induced porosity [74–77]. As also recently observed by Conte and co-workers [78], the volume variation associated with phase crystallization from a melt induced the formation of spherical intragranular pores in the glassy matrix. The concentration of anorthite around the coarse pores observed in Fig. 5Sb (supplementary materials) supports this hypothesis.

Fig. 12 illustrates the bodies under overfiring conditions, with the primary distinction being the increase in pore size. However, none of the WS bodies exhibit excessive bloating phenomena, likely due to a sort of stiffening of the microstructure resulting from the widespread and interconnected anorthite crystals (Fig. 6S, supplementary materials).

The color coordinates of the tiles at the gresification temperature are shown in Fig. 13, together with an image of the samples. The presence of limestone silt induced a slight lightning, with an increase in the L^* parameter. In fact, starting from L^* 68.3 of the benchmark, this value reached 70.7 to 72.6 for the other bodies, which also present lower a^* values, i.e. are less red. The effect of WS addition is different for b^* which increased, compared to B0, in WS4 and WS8, which exhibit a yellower tone, is the same in WF4 and decreases in WF8, with a colder tone. Above all, the WS addition determines the whitening of the bodies, already highlighted for anorthite-rich ceramics [35,38,40,67].

4. Conclusion

In this work, porcelain stoneware batches containing mining waste deriving from the washing of carbonatic aggregates were studied. Five bodies were formulated: one benchmark and four mixtures containing a high proportion of waste silt (4–8 wt%) as a straightforward replacement for feldspars, or in bodies with a complete redesign of the formulation, to align the chemical composition as closely as possible with that of the benchmark. The results from the laboratory-scale simulation of the industrial process demonstrated that the introduction of limestone silt induced an increase in the gresification temperature and a decrease in densification efficiency. This phenomenon is associated with the crystallization of anorthite during firing, which, to some extent, hinders densification and leads to significant crystallization-related porosity. At the same time, the formation of an anorthite network presumably “stiffens” the microstructure of the tile, preventing excessive bloating phenomena in overfiring conditions and increasing flexural strength.

The reformulation of the entire batch improved the technological properties of the fired tiles, particularly by achieving higher values of bulk density compared to bodies made with a simple substitution of feldspar. In any case, all tested ceramic bodies meet the standard requirements for porcelain stoneware (ISO 13600 [79]). The slightly

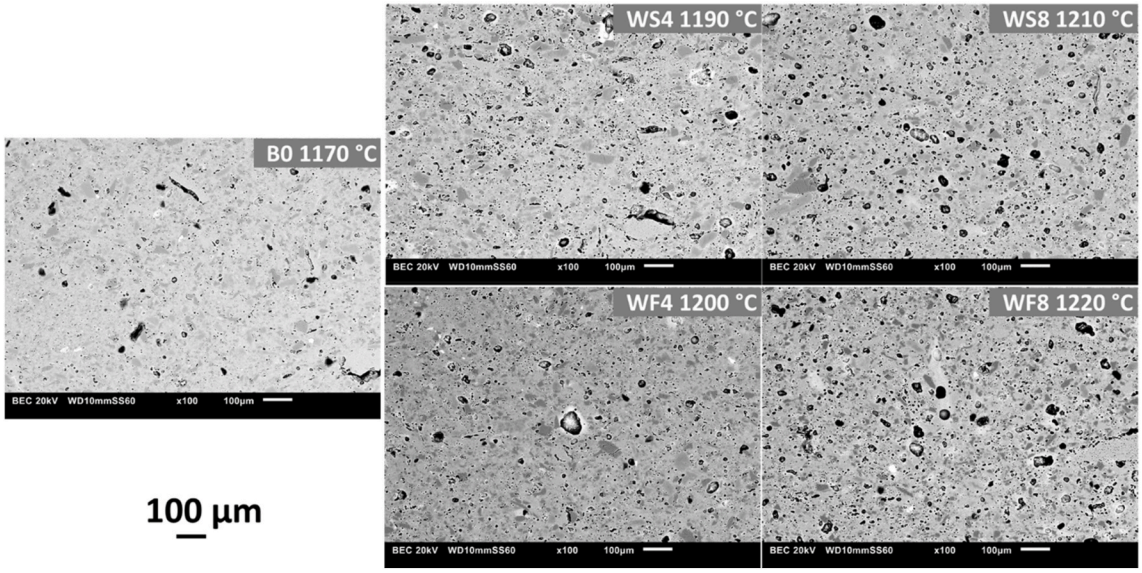

Fig. 11. SEM micrographs showing the microstructure of bodies fired at the gresification temperature.

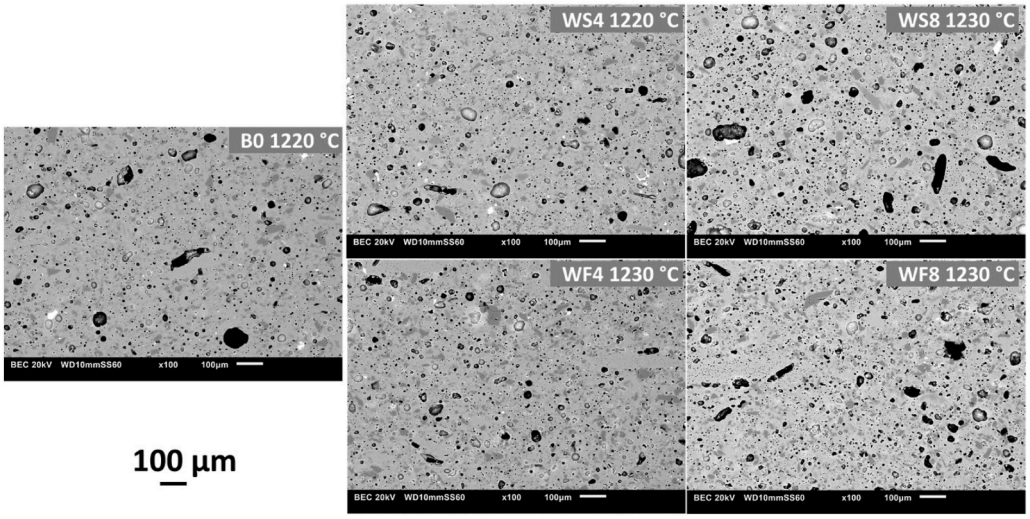

Fig. 12. SEM images showing the microstructure of bodies in overfiring conditions.

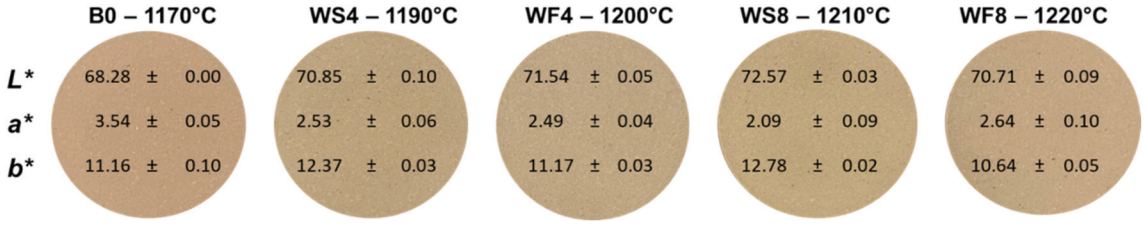

Fig. 13. Color of the tiles at the gresification temperature.

higher close porosity developed in the batches containing waste silt (with respect to the benchmark) is well tolerated in glazed porcelain stoneware rather than in technical porcelain stoneware. In the wide area of waste introduction into ceramic formulations, a proper re-engineering of porcelain stoneware batch can lead to promising results even with traditionally unfavorable materials. In this regard, a comprehensive model to predict waste behavior is auspicious but still requires efforts from scientific and industrial stakeholders. In addition, the decrease in quartz content associated with anorthite crystallization (due to the presence of limestone) observed in all fired bodies containing waste silt may contribute significantly to the ongoing debate in the ceramic industry on the lowering of quartz in finished products, directing research towards the use of sintering promoters as a means of limiting the presence of crystalline free silica.

CRediT authorship contribution statement

Riccardo Fantini: Writing – original draft, Methodology, Investigation, Formal analysis. **Sonia Conte:** Writing – review & editing, Writing – original draft, Methodology, Investigation, Formal analysis, Data curation, Conceptualization. **Chiara Molinari:** Writing – review & editing. **Chiara Zanelli:** Writing – review & editing, Funding acquisition. **Michele Dondi:** Writing – review & editing, Validation. **Maddalena Bernini:** Formal analysis. **Alessandro F. Gualtieri:** Writing – review & editing. **Rossella Arletti:** Writing – review & editing, Supervision, Funding acquisition.

Declaration of competing interest

The author Michele Dondi is an Editorial Board Member for this journal and was not involved in the editorial review or the decision to publish this article.

Acknowledgements

Our thanks go to CABE s.r.l. produzione, lavorazione e vendita inerti (Santarcangelo di Romagna, Rimini, Italy) for providing the samples for this study. We are also grateful to Dr. Simona Marchetti Dori and Dr. Simona Bigi for the granulometry and XRF analyses. This work was funded by the Project ECOSISTER (ECS_00000033) under the National Recovery and Resilience Plan (NRRP), Mission 04 Component 2 Investment 1.5 – Next Generation EU.

Appendix A. Supplementary data

Supplementary data to this article can be found online at https://doi.org/10.1016/j.ceramint.2025.11.373.

References

[1] L. Baraldi, World production and consumption of ceramic tiles, Ceramic World Review 153 (2023) 58–73.
[2] F. Andreola, L. Barbieri, I. Lancellotti, C. Leonelli, T. Manfredini, Recycling of industrial wastes in ceramic manufacturing: state of art and glass case studies, Ceram. Int. 42 (12) (2016) 13333–13338, https://doi.org/10.1016/j.ceramint.2016.05.205.
[3] C. Zanelli, S. Conte, C. Molinari, R. Soldati, M. Dondi, Waste recycling in ceramic tiles: a technological outlook, Resour. Conserv. Recycl. 168 (2021) 105289, https://doi.org/10.1016/j.resconrec.2020.105289.
[4] Directive 2006/21/EC of the European parliament and of the council of 15 March 2006 on the management of waste from extractive industries, Orkesterjournalen L 102 (11.4) (2006) 15–34.
[5] N. Careddu, G.A. Dino, S.W. Danielsen, R. Přikryl, Raw materials associated with extractive industry: an overview, Resour. Policy 59 (2018) 1–6.
[6] G. Bozzola, G.A. Dino, M. Fornaro, A. Lorenzi, Technological innovations and new products obtained from a virtuosos management of mining waste, in: 4th International Conference on Engineering for Waste and Biomass Valorisation, 2012, pp. 1–6. Nzihou A. and Castro F.
[7] G.A. Dino, P. Clemente, M. Lasagna, D.A. De Luca, Residual sludge from dimension stones: characterisation for their exploitation in civil and environmental

applications, Energy Proc. 40 (2013) 507–514, https://doi.org/10.1016/j.egypro.2013.08.058.
[8] M. Bozzola, S.G.M.M. Lorenzi, F. Dino, I residui dell'attività estrattiva: scarti da deposito o neominiere da valorizzare? Istituto Superiore per la Protezione e la Ricerca Ambientale, ISPRA-Settore Editoria (2014).
[9] N. Careddu, G.A. Dino, Reuse of residual sludge from stone processing: differences and similarities between sludge coming from carbonate and silicate stones—Italian experiences, Environ. Earth Sci. 75 (2016) 1–9.
[10] N. Careddu, G. Marras, G. Siotto, Recovery of sawdust resulting from marble processing plants for future uses in high value added products, J. Clean. Prod. 84 (2014) 533–539.
[11] G.A. Dino, N. Mehta, P. Rossetti, F. Ajmone-Marsan, D.A. De Luca, Sustainable approach towards extractive waste management: two case studies from Italy, Resour. Policy 59 (2018) 33–43.
[12] A. Cavallo, Serpentinitic waste materials from the dimension stone industry: characterization, possible reuses and critical issues, Resour. Policy 59 (2018) 17–23, https://doi.org/10.1016/j.resourpol.2018.08.003.
[13] L. Zichella, G.A. Dino, R. Bellopede, P. Marini, E. Padoan, I. Passarella, Environmental impacts, management and potential recovery of residual sludge from the stone industry: the piedmont case, Resour. Policy 65 (2020) 101562, https://doi.org/10.1016/j.resourpol.2019.101562.
[14] G. Bozzola, G.A. Dino, M. Fornaro, A. Lorenzi, Technological innovations and secondary raw materials obtained from virtuous management of wastes connected to mining activities: the examples of Gruppo Minerali Maffei s.p.a, Rend. line della Soc. Geol. Ital (2010) 519–520.
[15] F. Carranza, R. Romero, A. Mazuelos, N. Iglesias, Recovery of Zn from acid mine water and electric arc furnace dust in an integrated process, J. Environ. Manag. 165 (2016) 175–183.
[16] R.B. Gordon, Production residues in copper technological cycles, Resour. Conserv. Recycl. 36 (2002) 87–106.
[17] D. Medas, R. Cidu, G. De Giudici, F. Podda, Geochemical behaviour of rare earth elements in mining environments under non-acidic conditions, Procedia Earth Planet. Sci. 7 (2013) 578–581 (1878-5220) (2013).
[18] C. Jiang, S. Huang, G. Li, X. Zhang, X. Cheng, Formation of closed-pore foam ceramic from granite scraps, Ceram. Int. 44 (3) (2018) 3469–3471.
[19] M.N. Amin, K. Khan, M.U. Saleem, N. Khurram, M.U.K. Niazi, Aging and curing temperature effects on compressive strength of mortar containing lime stone quarry dust and industrial granite sludge, Materials 10 (6) (2017) 642.
[20] T. Ramos, A.M. Matos, B. Schmidt, J. Rio, J. Sousa-Coutinho, Granitic quarry sludge waste in mortar: effect on strength and durability, Constr. Build. Mater. 47 (2013) 1001–1009.
[21] M.M. Jordán, S. Pina, F. García-Orenes, M.B. Almendro-Candel, E. García-Sánchez, Environmental risk evaluation of the use of mine spoils and treated sewage sludge in the ecological restoration of limestone quarries, Environ. Geol. 55 (2008) 453–462, https://doi.org/10.1007/s00254-007-0991-4.
[22] G.A. Dino, M. Fornaro, E. Fornaro, S. Assone, D. Mainero, E. Corio, Quarry rehabilitation: first results of an experimental project about residual sludge bioremediation treatment, in: Order to Obtain Loam. Convegno MPES. Torino 20-22 Settembre 2006, 2006, pp. 292–297. ISBN 88-901342-4-0.
[23] G.A. Dino, M. Fornaro, E. Corio, E. Fornaro, Residual sludge management: a possible reuse as loam, in: The 10th IAEG Congress, Engineering geology for tomorrow's cities, Nottingham, United Kingdom, 6–10 September 2006, p. 10, 2006 b.
[24] P. Velumani, S. SenthilKumar, P.V. Premalatha, An Innovative Approach to Evaluate the Performance of sludge-incorporated Fly Ash Bricks, ASTM International, 2015.
[25] R. Bouachera, R. Kasimi, M. Ibnoussina, M. El Aoud, Y. Taha, H. El Boudour El Idrissi, R. Hakkou, The clayey quarry sludge from a waste to a valuable raw material for red ceramics, J. Mater. Cycles Waste Manag. 24 (3) (2022) 1047–1058.
[26] R. Sokolar, S. Grygarova, Utilization of waste quarry washing sludge for the production of dry pressed ceramic bodies, J. Ceram. Soc. Jpn. 121 (1409) (2013) 120–122.
[27] M. Loutou, R. Hakkou, R. Argane, M. Mansori, L. Grase, R. Svinka, G. Mezinskis, Clayey quarry sludges: thermal transformation, microstructure and technological properties, Waste Biomass Valoriz. 9 (2018) 1805–1815.
[28] G.A. Dino, I. Passarella, F. Ajmone Marsan, Quarry rehabilitation employing treated residual sludge from dimension stone working plant, Environ. Earth Sci. (2014), https://doi.org/10.1007/s12665-014-3895-0.
[29] G.A. Dino, P. Clemente, M. Lasagna, I. Passarella, F. Ajmone Marsan, D.A. De Luca, Industrial chance to recover residual sludge from dimension stones in civil and environmental applications, in: G. Lollino, A. Manconi, F. Guzzetti, M. Culshaw, P. Bubrowsky, F. Luino (Eds.), Engineering Geology for Society and Territory (Urban Geology, Sustainable Planning and Landscape Exploitation), vol. 5, Springer, Berlin, 2015, pp. 1309–1313, https://doi.org/10.1007/978-3-319-09048-1_250.
[30] G.A. Dino, S.W. Danielsen, C. Chiappino, C.J. Engelsen, Recycling of rock materials as part of sustainable aggregate production in Norway and Italy, Q. J. Eng. Geol. Hydrogeol. 50 (4) (2017) 412–416.
[31] V. Corinaldesi, G. Moriconi, T.R. Naik, Characterization of marble powder for its use in mortar and concrete, Constr. Build. Mater. 24 (1) (2010) 113–117.
[32] B.S. Sena da Fonseca, C. Galhano, A. Vilão, Utilization of Estremoz marbles sawing sludge in ceramic industry–Preliminary approach, Civ. Environ. Res. 3 (No.9) (2013).
[33] M. Galetakis, A. Soultana, A review on the utilisation of quarry and ornamental stone industry fine by-products in the construction sector, Constr. Build. Mater. 102 (2016) 769–781.
[34] P.K. Gautam, P. Kalla, R. Nagar, A.S. Jethoo, Laboratory investigation on use of quarry waste in open graded friction course, Resour. Policy 59 (2018) 62–67.
[35] S. Ke, X. Cheng, Y. Wang, Q. Wang, H. Wang, Dolomite, wollastonite and calcite as different CaO sources in anorthite-based porcelain, Ceram. Int. 39 (5) (2013) 4953–4960.
[36] C. Dagounaki, C. Sikalidis, A. Kassoli-Fournaraki, A. Tsirambides, The influence of carbonates on the technological properties of an industrial porcelain type body, Ind. Ceram. 29 (2009) 2.
[37] T.T. Mbakop, J.G.N. Deutou, L. Boubakar, N. Billong, U.C. Melo, E. Kamseu, V. M. Sglavo, Enhancing the crystallization phenomena and strength of porcelain stoneware: the role of CaO, J. Therm. Anal. Calorim. 144 (2021) 91–106.
[38] M. Lassinantti Gualtieri, E. Colombini, D. Mazzini, C. Alboni, T. Manfredini, C. Siligardi, The effect of alkaline Earth carbonates on the microstructure and mechanical properties of impermeable and lightweight ceramics, J. Eur. Ceram. Soc. 38 (16) (2018) 5563–5568.
[39] Q. Bao, W. Dong, J. Zhou, K. Liu, T. Zhao, Influence of calcite on the microstructure and sintering properties of the porcelain ceramic tiles at low temperature, J. Ceram. Soc. Jpn. 125 (12) (2017) 881–886.
[40] X. Cheng, S. Ke, Q. Wang, H. Wang, A. Shui, P. Liu, Fabrication and characterization of anorthite-based ceramic using mineral raw materials, Ceram. Int. 38 (4) (2012) 3227–3235.
[41] S. Kurama, E. Ozel, The influence of different CaO source in the production of anorthite ceramics, Ceram. Int. 35 (2) (2009) 827–830.
[42] C.T. Brasileiro, S. Conte, F. Contartesi, F.G. Melchiades, C. Zanelli, M. Dondi, A. O. Boschi, Effect of strong mineral fluxes on sintering of porcelain stoneware tiles, J. Eur. Ceram. Soc. 41 (11) (2021) 5755–5767.
[43] The map was extracted from the Geo-server of the Emilia Romagna region consulted through the MOKA system. https://servizimoka.regione.emilia-romagna.it/mokaApp/apps/geo/index.html (Access September 29th, 2025; in Italian).
[44] H.M. Rietveld, The rietveld method: a retrospection, Z. Kristallogr. Cryst. Mater. 225 (12) (2010) 545–547, https://doi.org/10.1524/zkri.2010.1356, 2010.
[45] A.F. Gualtieri, Accuracy of XRPD QPA using the combined Rietveld–RIR method, Appl. Crystallogr 33 (2) (2000) 267–278.
[46] T. Degen, M. Sadki, E. Bron, U. Konig, G. Nénert, The HighScore suite, Powder Diffr. 29 (2014), https://doi.org/10.1017/S0885715614000840.
[47] A.C. Larson, R.B. Von Dreele, General Structure Analysis System. Report LAUR 86–748, Los Alamos National Laboratory, New Mexico, USA, 2004.
[48] B.H. Toby, EXPGUI, a graphical user interface for GSAS, J. Appl. Crystallogr. 34 (2) (2001) 210–213.
[49] Soil Quality — Determination of Carbonate Content — Volumetric Method, 2021. ISO 10693:1995.
[50] Particle Size Analysis — Laser Diffraction Methods, 2025. ISO 13320:2020.
[51] Geotechnical Investigation and Testing — Laboratory Testing of Soil. Part 12: Determination of Liquid and Plastic Limits, 2023. ISO 17892-12:2018.
[52] G. Cultrone, C. Rodriguez-Navarro, E. Sebastian, O. Cazalla, M.J. De La Torre, Carbonate and silicate phase reactions during ceramic firing, European Journal Of Mineralogy-Stuttgart- 13 (3) (2001) 621–634.
[53] K. Traore, T.S. Kabre, P. Blanchart, Gehlenite and anorthite crystallisation from kaolinite and calcite mix, Ceram. Int. 29 (4) (2003) 377–383.
[54] M. Dondi, G. Guarini, S. Conte, C. Molinari, R. Soldati, C. Zanelli, Deposits, composition and technological behavior of fluxes for ceramic tiles, Period. Mineral. 88 (3) (2019).
[55] E. Sánchez, V. Sanz, E. Canas, J. Sales, K. Kayacı, M.U. Taşkıran, U.E. Anıl, Ş. Turk, Revisiting pyroplastic deformation. Application for porcelain stoneware tile bodies, J. Eur. Ceram. Soc. 39 (2019) 601–609.
[56] M. Dondi, M. Raimondo, C. Zanelli, Clays and bodies for ceramic tiles: reappraisal and technological classification, Appl. Clay Sci. 96 (2014) 91–109.
[57] C. Mugoni, M. Montorsi, C. Siligardi, F. Andreola, I. Lancellotti, E. Bernardo, L. Barbieri, Design of glass foams with low environmental impact, Ceram. Int. 41 (2015) 3400–3408.
[58] C. Molinari, C. Zanelli, L. Laghi, G. De Aloysio, M. Santandrea, G. Guarini, S. Conte, M. Dondi, Effect of scale-up on the properties of PCM-impregnated tiles containing glass scraps, Case Stud. Constr. Mater. 14 (2021) e00526.
[59] ASTM C958-92, Standard Test Method for Particle Size Distribution of Alumina or Quartz by X-Ray Monitoring of Gravity Sedimentation, 2022.
[60] ASTM C324-01, Standard Test Method for Free Moisture in Ceramic Whiteware Clays, 2022.
[61] ASTM C373-18, Standard Test Methods for Determination of Water Absorption and Associated Properties by Vacuum Method for Pressed Ceramic Tiles and Glass Tiles and Boil Method for Extruded Ceramic Tiles and Non-tile Fired Ceramic Whiteware Products, 2023.
[62] ISO 10545-16, Piastrelle Di Ceramica - Parte 16: Determinazione Di Piccole Differenze Di Colore, 2012.
[63] ASTM C648-20, Standard Test Method for Breaking Strength of Ceramic Tile, 2020.
[64] S. Conte, C. Zanelli, C. Molinari, G. Guarini, M. Dondi, Glassy wastes as feldspar substitutes in porcelain stoneware tiles: thermal behaviour and effect on sintering process, Mater. Chem. Phys. 256 (2020) 123613.
[65] S. Conte, C. Molinari, M. Ardit, G. Cruciani, M. Dondi, C. Zanelli, Porcelain versus porcelain stoneware: so close, So different. Sintering kinetics, phase evolution, and vitrification paths, Materials 16 (1) (2022) 171.
[66] S. Conte, C. Molinari, M. Ardit, D. Giordano, M. Dondi, C. Zanelli, Vitrification Paths in Porcelain Stoneware: Dependence on Bulk Chemical Composition and Effect on Sintering Behaviour, preparation, 2025.

[67] G. Çigdemir, A. Kara, F. Kara, Effect of Earth alkaline oxides on firing behaviour of porcelain stoneware, Ind. Ceram. 30 (2010) 3.
[68] S. Conte, C. Zanelli, M. Ardit, G. Cruciani, M. Dondi, Phase evolution during reactive sintering by viscous flow: disclosing the inner workings in porcelain stoneware firing, J. Eur. Ceram. Soc. 40 (4) (2020) 1738–1752.
[69] M. Dondi, G. Ercolani, G. Guarini, M. Marsigli, I. Venturi, Evolution of the microstructure during firing of bodies for porous tiles, Ceramurgia 25 (6) (1995) 301–314.
[70] C. Molinari, S. Conte, M. Dondi, C. Zanelli, Content of crystalline silica phases in porcelain stoneware, Open Ceramics 19 (2024) 100650, https://doi.org/10.1016/j.oceram.2024.100650.
[71] Š. Csáki, F. Lukáč, T. Húlan, J. Veverka, M. Knapek, Preparation of anorthite ceramics using SPS, J. Eur. Ceram. Soc. 41 (8) (2021) 4618–4624, https://doi.org/10.1016/j.jeurceramsoc.2021.03.004.
[72] F. González-García, V. Romero-Acosta, G. García-Ramos, M. González-Rodríguez, Firing transformations of mixtures of clays containing illite, kaolinite and calcium carbonate used by ornamental tile industries, Appl. Clay Sci. 5 (4) (1990) 361–375.
[73] P.H. Ribbe, Chemistry, structure and nomenclature of feldspars, in: ISBN 0-939950-14-6, Feldspar Mineralogy, Reviews in Mineralogy, vol. 2, Mineralogical Societyof America, Washington, 1983, pp. 1–20.
[74] A. Karamanov, M. Pelino, Sinter-crystallisation in the diopside–albite system Part I. Formation of induced crystallisation porosity, J. Eur. Ceram. Soc. 26 (2006) 2511–2517.
[75] A. Karamanov, M. Pelino, Induced crystallization porosity and properties of sintered diopside and wollastonite glass-ceramics, J. Eur. Ceram. Soc. 28 (2008) 555–562.
[76] V.M. Fokin, A.S. Abyzov, J.W.P. Schmelzer, E.D. Zanotto, Stress induced pore formation and phase selection in a crystallizing stretched glass, J. Non-Cryst. Solids 356 (2010) 1679–1688.
[77] O. Peitl, E.D. Zanotto, K. Heide, Crystallization-triggered bubbles in glass-ceramics, Ceram. Int. 46 (2020) 22513–22520.
[78] S. Conte, R. Fantini, R. Arletti, C. Molinari, M. Dondi, C. Zanelli, A.F. Gualtieri, Sintering mechanisms, phase transformations and microstructure of porcelain stoneware containing thermally inertized man-made vitreous fibres, J. Eur. Ceram. Soc. 45 (2025) 117230, https://doi.org/10.1016/j.jeurceramsoc.2025.117230.
[79] ISO 13006, Ceramic tiles—definitions, Classification, Characteristics and Marking, International Organization for Standardization, 2018.